

# Pyramid Vision Transformer: A Versatile Backbone for Dense Prediction without Convolutions

Wenhai Wang<sup>1</sup>, Enze Xie<sup>2</sup>, Xiang Li<sup>3</sup>, Deng-Ping Fan<sup>4</sup>,  
Kaitao Song<sup>3</sup>, Ding Liang<sup>5</sup>, Tong Lu<sup>1</sup>, Ping Luo<sup>2</sup>, Ling Shao<sup>4</sup>

<sup>1</sup>Nanjing University <sup>2</sup>The University of Hong Kong

<sup>3</sup>Nanjing University of Science and Technology <sup>4</sup>IIAI <sup>5</sup>SenseTime Research

wangwenhai362@smail.nju.edu.cn, lutong@nju.edu.cn

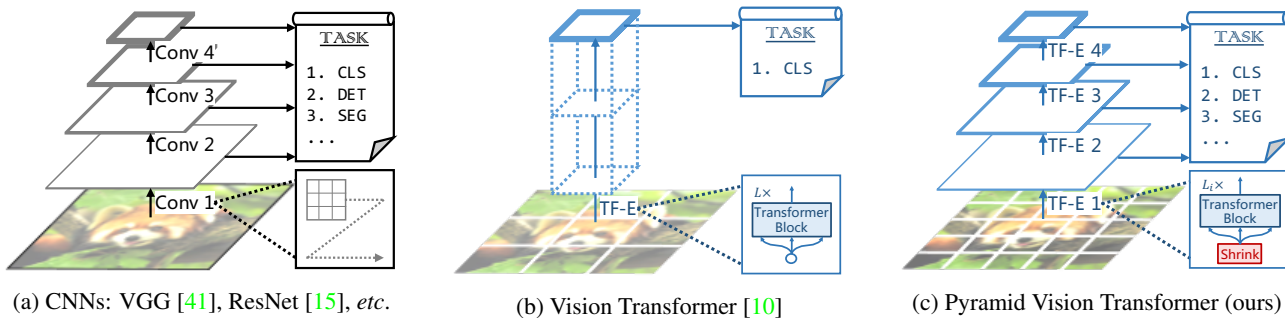


Figure 1: **Comparisons of different architectures**, where “Conv”, and “TF-E”, represent convolution, and Transformer Encoder, respectively. (a) shows that many CNN backbones use pyramid structure for dense prediction tasks such as object detection (DET), semantic and instance segmentation (SEG). (b) shows that the recently proposed Vision Transformer (ViT) [10] is a “columnar” structure specially-designed for image classification (CLS). (c) illustrates that by incorporating the pyramid structure from CNNs, we present Pyramid Vision Transformer (PVT), which can be used as a versatile backbone for many computer vision tasks, broadening the scope and impact of ViT. Moreover, our experiments also show that PVT can be easily combined with DETR [4] to build an end-to-end object detection system without convolutions and hand-crafted components such as dense anchors and non-maximum suppression (NMS).

## Abstract

Although using convolutional neural networks (CNNs) as backbones achieves great successes in computer vision, this work investigates a simple backbone network useful for many dense prediction tasks without convolutions. Unlike the recently-proposed Transformer model (e.g., ViT) that is specially designed for image classification, we propose Pyramid Vision Transformer (PVT), which overcomes the difficulties of porting Transformer to various dense prediction tasks. PVT has several merits compared to prior arts. (1) Different from ViT that typically has low-resolution outputs and high computational and memory cost, PVT can be not only trained on dense partitions of the image to achieve high output resolution, which is important for dense prediction, but also using a progressive shrinking pyramid to reduce computations of large feature maps. (2) PVT inherits the advantages from both CNN and Transformer, making it a unified backbone in various vision tasks without

convolutions by simply replacing CNN backbones. (3) We validate PVT by conducting extensive experiments, showing that it boosts the performance of many downstream tasks, e.g. object detection, semantic and instance segmentation. For example, with a comparable number of parameters, RetinaNet+PVT achieves 40.4 AP on the COCO dataset, surpassing RetinaNet+ResNet50 (36.3 AP) by 4.1 absolute AP (see Figure 2). We hope PVT could serve as an alternative and useful backbone for pixel-level predictions and facilitate future researches. Code is available at <https://github.com/whai362/PVT>.

## 1. Introduction

Convolution Neural Network (CNN) achieves remarkable successes in computer vision, and becomes a versatile and dominating method in almost all tasks of computer vision [9, 28, 11, 63, 41, 15, 56, 36, 14, 27, 7, 21]. Nevertheless, this work is trying to explore new versatile backbone

network without convolutions. We investigate an alternative model beyond CNN for the tasks of dense predictions such as object detection, semantic and instance segmentation, other than image classification.

Inspired by the success of Transformer [51] in natural language processing (NLP), many researchers are trying to explore applications of Transformer in computer vision. For example, some works [4, 64, 55, 43, 17] model the vision task as a dictionary lookup problem with learnable queries, and use the Transformer decoder as a task-specific head on the top of the CNN backbone, such as VGG [41] and ResNet [15]. While some prior arts have incorporated the attention modules [53, 35, 61] into CNNs, as far as we know, exploring a clean and convolution-free Transformer backbone to address dense prediction tasks in computer vision is rarely studied.

Recently, Dosovitskiy *et al.* [10] employs Transformer for image classification. This is an interesting and meaningful attempt to replace the CNN backbone by a convolution-free model. As shown in Figure 1 (b), ViT has a columnar structure with coarse image patches (*i.e.*, dividing image with a large patch size) as input<sup>1</sup>. Although ViT is applicable to image classification, **it is challenging to be directly adapted to pixel-level dense predictions**, *e.g.*, object detection and segmentation, because (1) its output feature map has only a single scale with low resolution and (2) its computations and memory cost are relatively high even for common input image size (*e.g.*, shorter edge of 800 pixels in COCO detection benchmark).

To compensate the above limitations, this work proposes a convolution-free backbone network using Transformer model, termed Pyramid Vision Transformer (PVT), which can serve as a versatile backbone in many downstream tasks, including image-level prediction as well as pixel-level dense predictions. Specifically, as illustrated in Figure 1 (c), different from ViT, PVT overcomes the difficulties of conventional Transformer by (1) taking fine-grained image patches (*i.e.*,  $4 \times 4$  per patch) as input to learn high-resolution representation, which is essential for dense prediction tasks, (2) introducing a progressive shrinking pyramid to reduce the sequence length of Transformer when the depth of network is increased, significantly reducing the computational consumption, and (3) adopting a spatial-reduction attention (SRA) layer to further reduce the resource cost to learn high-resolution feature maps.

Overall, the proposed PVT possesses the following merits. Firstly, compared to the conventional CNN backbones (see Figure 1 (a)) where the receptive field increases when the depth increases, PVT always produces a global recep-

<sup>1</sup>Due to resource constraints, ViT cannot use fine-grained image patches (*e.g.*,  $4 \times 4$  per patch) as input, and can only receive coarse patches (*e.g.*,  $32 \times 32$  per patch) as input, which leads to its low output resolution (*e.g.*, 32-stride).

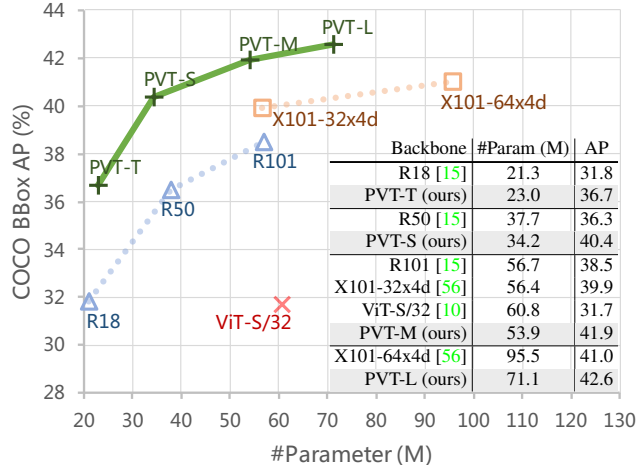


Figure 2: **Performance comparison on COCO val2017 of different backbones using RetinaNet for object detection.** We see that when the number of parameters among different models are comparable, the PVT variants significantly outperform their corresponding counterparts in COCO such as ResNets (R) [15], ViT [10] and ResNeXts (X) [56]. For instance, with comparable numbers of parameters, PVT-S outperforms R50 by 4.1 AP (40.4 vs. 36.3), where “T”, “S”, “M” and “L” denote our PVT models with tiny, small, medium and large size. We also see that the original ViT models could be limited in object detection.

tive field (by attentions among all small patches), which is more suitable for detection and segmentation than CNNs’ local receptive field. Secondly, compared to ViT (see Figure 1 (b)), due to the advance of the pyramid structure, our method is easier to be plugged into many representative dense prediction pipelines, *e.g.*, RetinaNet [27] and Mask R-CNN. Thirdly, with PVT, we can build a convolution-free pipeline by combining PVT with other Transformer decoders designed for different tasks, such as PVT+DETR [4] for object detection. For example, to the best of our knowledge, *our experiments present the first end-to-end object detection pipeline, PVT+DETR*, which is entirely convolution-free. It achieves 34.7 on the COCO val2017, outperforming the original DETR based on ResNet50.

The main **contributions** of this work are listed below.

- We propose Pyramid Vision Transformer (PVT), which is the first backbone designed for various pixel-level dense prediction tasks without convolutions. Combining PVT and DETR, we can build an end-to-end object detection system without convolutions and hand-crafted components such as dense anchors and non-maximum suppression (NMS).
- We overcome many difficulties when porting Transformer to dense pixel-level predictions, by designing

progressive shrinking pyramid and spatial-reduction attention (SRA), which are able to reduce the resource consumption of using Transformer, making PVT flexible to learn multi-scale and high-resolution feature maps.

- We verify PVT by applying it to many different tasks, *e.g.*, image classification, object detection, and semantic segmentation, and compare it with the well-designed ResNets [15] and ResNeXts [56]. As shown in Figure 2, we see that PVT with different numbers of parameters can consistently improve performance compared to prior arts. For example, RetinaNet+PVT-Small achieves 40.4 AP on COCO va12017, outperforming RetinaNet+ResNet50 by 4.1 AP (40.4 vs. 36.3). Moreover, RetinaNet+PVT-Large achieves 42.6 AP, which is 1.6 better than RetinaNet+ResNeXt101-64x4d, as well as reducing its number of parameters by 30%.

## 2. Related Work

### 2.1. Convolutional Backbones in Computer Vision

Convolutional block is the work-horse of deep neural networks in visual recognition. The standard and fundamental convolutional block was first introduced in [23] to distinguish hand-writing numbers. The block contains convolutional kernels with a certain receptive field that captures favorable visual context. To introduce the translation equivariance, the weights of convolutional kernels are shared over the entire image space. With the rapid development of the computational resources (*e.g.*, GPUs), the successful training for a stack of a few convolutional blocks [22, 41] on large-scale image classification dataset (*e.g.*, ImageNet [38]) becomes possible. GoogLeNet [46] demonstrated that a convolutional operator containing multiple kernel paths can achieve very competitive performance. The effectiveness of multi-path convolutional block was further validated in Inception series [47, 45], ResNeXt [56], DPN [8], MixNet [52] and SKNet [24]. Further, ResNet [15] proposed skip connections in convolutional blocks, which makes very deep networks possible and has impressive effects in the field of computer vision. DenseNet [18] introduced densely connected topology, which connects each convolutional block to its previous blocks. More recent advances can be found in recent survey/review papers [20, 40].

### 2.2. Dense Prediction Tasks

**Preliminary.** The dense prediction task aims to perform pixel-level classification or regression on the feature map. Object detection and semantic segmentation are two representative dense prediction tasks.

**Object Detection.** In the deep learning era, CNN [23] has become the dominant framework for object detection, which includes single-stage detectors (*e.g.*, SSD [30], RetinaNet [27], FCOS [49], GFL [25], PolarMask [54] and OneNet [42]) and multiple-stage detectors (Faster R-CNN [36], Mask R-CNN [14], Cascade R-CNN [3] and Sparse R-CNN [44]). Most of these popular object detectors are built on high-resolution or multi-scale feature maps, to obtain a good detection performance. Recently, DETR [4] and deformable DETR [64] combine the CNN backbone and the Transformer decoder to build an end-to-end object detector. Like the previous CNN-based detectors, they also require high-resolution or multi-scale feature maps for accurate object detection.

**Semantic Segmentation.** CNN also plays an important role in semantic segmentation. In the early stage, FCN [31] introduced fully convolutional architectures to generate a spatial segmentation map for a given image of any size. After that, deconvolution operation was introduced by Noh *et al.* [34] and achieved impressive performance on PASCAL VOC 2012 dataset [39]. Inspired by FCN, U-Net [37] is proposed for especially the medical image segmentation domain, which bridges the information flow between corresponding low-level and high-level feature maps with the same spatial sizes. To explore richer global context representation, Zhao *et al.* [62] designs a pyramid pooling module over various pooling scales, and Kirillov *et al.* [21] develop a lightweight segmentation head termed Semantic FPN, based on FPN [26]. DeepLab family [6, 29] applies the dilated convolution to enlarge the receptive field while keeping the feature map resolution. Similar to object detection methods, semantic segmentation methods also rely on high-resolution or multi-scale feature maps.

### 2.3. Self-Attention and Transformer in Vision

As convolutional filter weights are usually fixed after training, it is inflexible for them to adapt dynamically to input variation. Therefore, many methods have been proposed to alleviate this problem via using self-attention operations. The non-local block [53] attempted to model long-range dependencies in both space and time, which is shown beneficial for accurate video classification. Despite its success, the non-local operator suffers from the high memory and computation cost. Criss-cross [19] further reduced the complexity by generating sparse attention maps only through the criss-cross path. Ramachandran *et al.* [35] proposed stand-alone self-attention was proposed to replace convolutional layers with local self-attention units. AANet [2] achieves competitive results when combining the self-attention and convolutional operations. DETR [4] utilize the Transformer decoder to model object detection as an end-to-end dictionary lookup problem with learn-

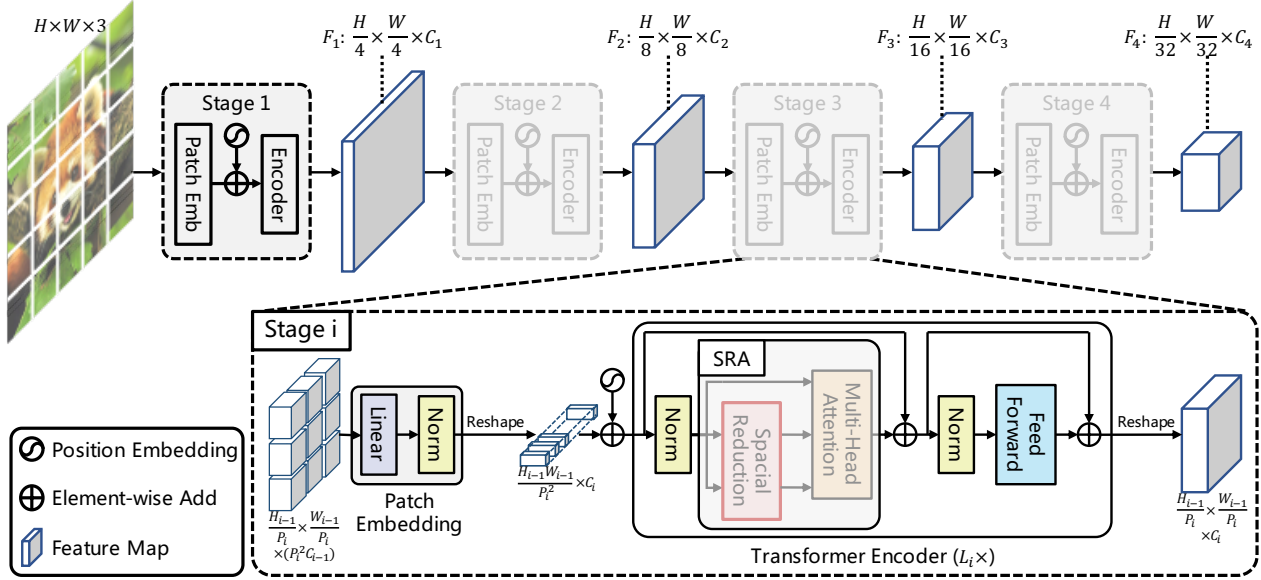


Figure 3: **Overall architecture of the proposed Pyramid Vision Transformer (PVT).** The entire model is divided into four stages, and each stage is comprised of a patch embedding layer, and a  $L_i$ -layer Transformer encoder. Following the pyramid structure, the output resolution of the four stages progressively shrinks from 4-stride to 32-stride.

able queries, successfully removing the hand-crafted process such as Non-Maximal Suppression (NMS). Based on DETR, deformable DETR [64] further introduces a deformable attention layer to focus on a sparse set of contextual elements which obtains fast convergence and better performance. Recently, Vision Transformer (ViT) [10] employs a pure Transformer [51] model to make image classification by treating an image as a sequence of patches. DeiT [50] further extends ViT by using a novel distillation approach. Different from previous methods, this work try to introduce the pyramid structure into Transformer and design a pure Transformer backbone for dense prediction tasks.

### 3. Pyramid Vision Transformer (PVT)

#### 3.1. Overall Architecture

Our goal is to introduce the pyramid structure into Transformer, so that it can generate multi-scale feature maps for dense prediction tasks (*e.g.*, object detection and semantic segmentation). An overview of PVT is depicted in Figure 3. Similar to CNN backbones [15], our method has four stages that generate feature maps of different scales. All stages share a similar architecture, which consists of a patch embedding layer and  $L_i$  Transformer encoder layers.

In the first stage, given an input image with the size of  $H \times W \times 3$ , we first divide it into  $\frac{HW}{4^2}$  patches<sup>2</sup>, and the size

<sup>2</sup>Same as ResNet, we keep the highest resolution of our output feature map at 4-stride.

of each patch is  $4 \times 4 \times 3$ . Then, we feed the flattened patches to a linear projection and get embedded patches with size of  $\frac{HW}{4^2} \times C_1$ . After that, the embedded patches along with position embedding pass through a Transformer encoder with  $L_1$  layer, and the output is reshaped to a feature map  $F_1$ , and its size is  $\frac{H}{4} \times \frac{W}{4} \times C_1$ . In the same way, using the feature map from the prior stage as input, we obtain the following feature maps  $F_2$ ,  $F_3$ , and  $F_4$ , whose strides are 8, 16, and 32 pixels with respect to the input image. With the feature pyramid  $\{F_1, F_2, F_3, F_4\}$ , our method can be easily applied to most downstream tasks, including image classification, object detection, and semantic segmentation.

#### 3.2. Feature Pyramid for Transformer

Unlike CNN backbone networks [15] that use convolution stride to obtain multi-scale feature maps, our PVT use *progressive shrinking strategy* to control the scale of feature maps by patch embedding layers.

Here, we denote the patch size of the  $i$ -th stage as  $P_i$ . At the beginning of the stage  $i$ , we first evenly divide the input feature map  $F_{i-1} \in \mathbb{R}^{H_{i-1} \times W_{i-1} \times C_{i-1}}$  into  $\frac{H_{i-1}W_{i-1}}{P_i^2}$  patches, and then each patch is flattened and projected to a  $C_i$ -dim embedding. After the linear projection, the shape of the embedded patches can be viewed as  $\frac{H_{i-1}}{P_i} \times \frac{W_{i-1}}{P_i} \times C_i$ , where the height and width are  $P_i$  times smaller than the input.

In this way, we can flexibly adjust the scale of the feature map in each stage, making it possible to construct a feature pyramid for Transformer.

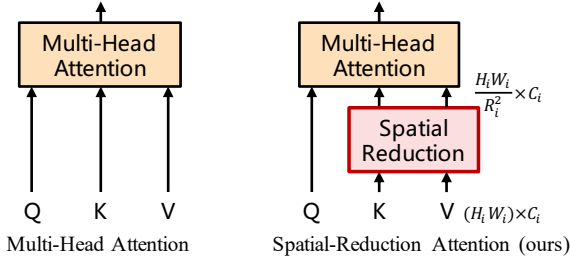


Figure 4: **Multi-head attention (MHA) vs. spatial-reduction attention (SRA)**. With spatial-reduction operation, the computational/memory cost of our SRA could be much lower than that of MHA, so our SRA is more friendly to high-resolution feature maps.

### 3.3. Transformer Encoder

For the Transformer encoder in the stage  $i$ , it has  $L_i$  encoder layers, and each encoder layer is composed of an attention layer and a feed-forward layer [51]. Since our method needs to process high-resolution (*e.g.*, 4-stride) feature maps, we propose a spatial-reduction attention (SRA) layer to replace the traditional multi-head attention (MHA) layer [51] in the encoder.

Similar to MHA, our SRA also receives a query  $Q$ , a key  $K$ , and a value  $V$  as input, and outputs a refined feature. The difference is that our SRA will reduce the spatial scale of  $K$  and  $V$  before the attention operation as shown in Figure 4, which largely reduces the computation/memory overhead. Details of SRA in the stage  $i$  can be formulated as follows:

$$\text{SRA}(Q, K, V) = \text{Concat}(\text{head}_0, \dots, \text{head}_{N_i})W^O, \quad (1)$$

$$\text{head}_j = \text{Attention}(QW_j^Q, \text{SR}(K)W_j^K, \text{SR}(V)W_j^V), \quad (2)$$

where  $W_j^Q \in \mathbb{R}^{C_i \times d_k}$ ,  $W_j^K \in \mathbb{R}^{C_i \times d_{\text{head}}}$ ,  $W_j^V \in \mathbb{R}^{C_i \times d_{\text{head}}}$ , and  $W^O \in \mathbb{R}^{h_i \times d_{\text{head}}}$  are parameters of linear projections.  $N_i$  is the head number of the Transformer encoder in the stage  $i$ . Therefore, the dimension of each head  $d_{\text{head}}$  is equal to  $\frac{C_i}{N_i}$ .  $\text{SR}(\cdot)$  is the spatial-reduction operation, which is defined as:

$$\text{SR}(\mathbf{x}) = \text{Norm}(\text{Reshape}(\mathbf{x}, R_i)W^S). \quad (3)$$

Here,  $R_i$  denotes the reduction ratio of the attention layers in the stage  $i$ .  $\text{Reshape}(\mathbf{x}, R_i)$  is the operation of reshaping the input  $\mathbf{x} \in \mathbb{R}^{(H_i W_i) \times C_i}$  to the sequence with the size of  $\frac{H_i W_i}{R_i^2} \times (R_i^2 C_i)$ .  $W^S \in \mathbb{R}^{(R_i^2 C_i) \times C_i}$  is a linear projection that reduces the dimension of input sequence to  $C_i$ .  $\text{Norm}(\cdot)$  refers to layer normalization [1]. Same as Transformer [51],

$\text{Attention}(\cdot)$  is the attention operation that is calculated as:

$$\text{Attention}(\mathbf{q}, \mathbf{k}, \mathbf{v}) = \text{Softmax}\left(\frac{\mathbf{q}\mathbf{k}^T}{\sqrt{d_{\text{head}}}}\right)\mathbf{v}. \quad (4)$$

Through these formulas, we can figure out that the computational/memory costs of our  $\text{Attention}(\cdot)$  operation is  $R_i^2$  times lower than that of MHA, and thus it can handle larger input feature maps/sequences with limited resources.

### 3.4. Model Details

In summary, the hyper parameters of our method are listed as follows:

- $P_i$ : the patch size of the stage  $i$ ;
- $C_i$ : the channel number of the output of the stage  $i$ ;
- $L_i$ : the number of encoder layers in the stage  $i$ ;
- $R_i$ : the reduction ratio of the SRA in the stage  $i$ ;
- $N_i$ : the head number of the SRA in the stage  $i$ ;
- $E_i$ : the expansion ratio of the feed-forward layer [51] in the stage  $i$ ;

Following the design rules of ResNet [15], we (1) use small output channel numbers in shallow stages; and (2) concentrate the major computation resource in intermediate stages.

To provide instances for discussion, we describe a series of PVT models with different scales, namely PVT-Tiny, -Small, -Medium, and -Large, in Table 1. More details of employing these models in specific downstream tasks will be introduced in Section 4.

### 3.5. Discussion

The most related work to our method is ViT [10]. Here we discuss in detail the relationship and differences between them.

Both PVT and ViT are pure Transformer models without convolution operation. The main difference between them is the pyramid structure. Similar to the traditional Transformer [51], the length of ViT’s output sequence is the same as the input, which means that the output of ViT is single-scale (see Figure 1 (b)). Moreover, due to the limited resource., the output of ViT is coarse-grained (*e.g.*, the patch size is 16 or 32 pixels), and thus its output resolution is relatively low (*e.g.*, 16-stride or 32-stride). As a result, it is difficult to directly apply ViT in dense prediction tasks that require high-resolution or multi-scale feature maps.

Our PVT breaks the routine of Transformer by introducing a progressive shrinking pyramid. It can generate multi-scale feature maps like a traditional CNN backbone. In addition, we also designed a simple but effective attention layer—SRA, to process high-resolution feature maps and reduce computation/memory costs. Benefiting from the above designs, our method has the following advantages over ViT: 1) more flexible—can generate feature maps of different scales, channels in differ-

	Output Size	Layer Name	PYT-Tiny	PYT-Small	PYT-Medium	PYT-Large
Stage 1	$\frac{H}{4} \times \frac{W}{4}$	Patch Embedding	$P_1 = 4; C_1 = 64$			
		Transformer Encoder	$\begin{matrix} R_1 = 8 \\ N_1 = 1 \\ E_1 = 8 \end{matrix} \times 2$	$\begin{matrix} R_1 = 8 \\ N_1 = 1 \\ E_1 = 8 \end{matrix} \times 3$	$\begin{matrix} R_1 = 8 \\ N_1 = 1 \\ E_1 = 8 \end{matrix} \times 3$	$\begin{matrix} R_1 = 8 \\ N_1 = 1 \\ E_1 = 8 \end{matrix} \times 3$
Stage 2	$\frac{H}{8} \times \frac{W}{8}$	Patch Embedding	$P_2 = 2; C_2 = 128$			
		Transformer Encoder	$\begin{matrix} R_2 = 4 \\ N_2 = 2 \\ E_2 = 8 \end{matrix} \times 2$	$\begin{matrix} R_2 = 4 \\ N_2 = 2 \\ E_2 = 8 \end{matrix} \times 3$	$\begin{matrix} R_2 = 4 \\ N_2 = 2 \\ E_2 = 8 \end{matrix} \times 3$	$\begin{matrix} R_2 = 4 \\ N_2 = 2 \\ E_2 = 8 \end{matrix} \times 8$
Stage 3	$\frac{H}{16} \times \frac{W}{16}$	Patch Embedding	$P_3 = 2; C_3 = 320$			
		Transformer Encoder	$\begin{matrix} R_3 = 2 \\ N_3 = 5 \\ E_3 = 4 \end{matrix} \times 2$	$\begin{matrix} R_3 = 2 \\ N_3 = 5 \\ E_3 = 4 \end{matrix} \times 6$	$\begin{matrix} R_3 = 2 \\ N_3 = 5 \\ E_3 = 4 \end{matrix} \times 18$	$\begin{matrix} R_3 = 2 \\ N_3 = 5 \\ E_3 = 4 \end{matrix} \times 27$
Stage 4	$\frac{H}{32} \times \frac{W}{32}$	Patch Embedding	$P_4 = 2; C_4 = 512$			
		Transformer Encoder	$\begin{matrix} R_4 = 1 \\ N_4 = 8 \\ E_4 = 4 \end{matrix} \times 2$	$\begin{matrix} R_4 = 1 \\ N_4 = 8 \\ E_4 = 4 \end{matrix} \times 3$	$\begin{matrix} R_4 = 1 \\ N_4 = 8 \\ E_4 = 4 \end{matrix} \times 3$	$\begin{matrix} R_4 = 1 \\ N_4 = 8 \\ E_4 = 4 \end{matrix} \times 3$

Table 1: **Detailed settings of PVT series.** The design follows the two rules of ResNet [15]: (1) with the growth of network depth, the hidden dimension gradually increases, and the output resolution progressively shrinks; (2) the major computation resource is concentrated in Stage 3.

ent stages; 2) more versatile—can be easily plugged and played in most downstream task models; 3) more friendly to computation/memory—can process the feature map with higher resolution.

## 4. Applied to Downstream Tasks

### 4.1. Image-Level Prediction

Image classification is the most representative task of image-level prediction. Following ViT [10] and DeiT [50], we append a learnable classification token to the input of the last stage, and then use a fully connected layer to make classification on the top of the classification token.

### 4.2. Pixel-Level Dense Prediction

In addition to image-level prediction, dense prediction that requires performing pixel-level classification or regression on the feature map is also often seen in downstream tasks. Here, we discuss two typical tasks, namely object detection, and semantic segmentation.

**Object Detection.** We apply our PVT models to two representative object detection methods, namely RetinaNet [27] and Mask R-CNN [14]. RetinaNet is a widely-used single-stage detector, and Mask R-CNN is one of the mainstream two-stage instance segmentation frameworks. The implementation details are listed as follows: (1) Same as ResNet, we directly use the output feature pyramid  $\{F_1, F_2, F_3, F_4\}$  as the input of FPN [26], and then the refined feature maps are fed to the follow-up detection or in-

stance segmentation head. (2) In object detection, the input can be an arbitrary shape, so the position embeddings pre-trained on ImageNet may no longer be meaningful. Therefore, we perform bilinear interpolation on the pre-trained position embeddings according to the input image. (3) During the training of the detection model, all layers in PVT will not be frozen.

**Semantic Segmentation.** We choose Semantic FPN [21] as the baseline, which is a simple segmentation method without special operations (*e.g.*, dilated convolution). Therefore, using it as the baseline can well examine the original effectiveness of backbones. Similar to the implementation in target detection, we feed the feature pyramid directly to the semantic FPN, and use bilinear interpolation to resize the pre-trained position embedding.

## 5. Experiments

We compare our PVT with the two most representative CNN backbones, namely ResNet [15], and ResNeXt [56], which are widely used in benchmarks of many downstream tasks.

### 5.1. Image Classification

**Experiment Settings.** We perform image classification experiments on the ImageNet dataset. The ImageNet 2012 dataset [38] comprises 1.28 million training images and 50K validation images from 1,000 categories. We train models on the training set, and report the top-1 error on the validation set. For a fair comparison, we follow DeiT [50]

Method	#Param (M)	GFLOPs	Top-1 (%)
R18* [15]	11.7	1.8	30.2
R18 [15]	11.7	1.8	31.5
DeiT-Tiny/16 [50]	5.7	1.3	27.8
PVT-Tiny (ours)	13.2	1.9	24.9
R50* [15]	25.6	4.1	23.9
R50 [15]	25.6	4.1	21.5
X50-32x4d* [56]	25.0	4.3	22.4
X50-32x4d [56]	25.0	4.3	20.5
DeiT-Small/16 [50]	22.1	4.6	20.1
PVT-Small (ours)	24.5	3.8	20.2
R101* [15]	44.7	7.9	22.6
R101 [15]	44.7	7.9	20.2
X101-32x4d* [56]	44.2	8.0	21.2
X101-32x4d [56]	44.2	8.0	19.4
ViT-Small/16 [10]	48.8	9.9	19.2
PVT-Medium (ours)	44.2	6.7	18.8
X101-64x4d* [56]	83.5	15.6	20.4
X101-64x4d [56]	83.5	15.6	18.5
ViT-Base/16 [10]	86.6	17.6	18.2
DeiT-Base/16 [50]	86.6	17.6	18.2
PVT-Large (ours)	61.4	9.8	18.3

Table 2: **Image classification performance on the ImageNet validation set.** “Top-1” denotes the top-1 error rate. “#Param” refers to the number of parameters. “GFLOPs” is calculated under the input scale of  $224 \times 224$ . “\*” indicates the performance of the method trained with the strategy in its original paper.

to perform the random-size cropping to  $224 \times 224$ , random horizontal flipping [46], and mixup [59] for data augmentation. Label-smoothing regularization [47] is used during training. We use AdamW [33] with the momentum of 0.9, a mini-batch size of 128, and a weight decay of  $5 \times 10^{-2}$  by default. The initial learning rate is set to  $1 \times 10^{-3}$  and decreases following the cosine schedule [32]. All models are trained for 300 epochs from scratch on 8 V100 GPUs. To benchmark, we apply a center crop on the validation set, where  $224 \times 224$  pixels are cropped for evaluating the recognition accuracy.

**Results.** In Table 2, we find that our PVT models are superior to conventional CNN backbones under similar parameter numbers and computation budgets. For example, when the GFLOPs are roughly similar, the top-1 error of PVT-Small reaches 20.2, which is 1.3 higher than that of ResNet50 [15] (21.5). Meanwhile, under similar or relatively lower complexity, our PVT family archives performance comparable (*i.e.*, 18.2 vs. 18.3) to the recently proposed Transformer-based models, such as ViT [10] and DeiT [50]. This result is within expectations, because the

pyramid structure may be beneficial to dense prediction tasks, but the gains it brings to image classification are limited.

Note that, ViT and DeiT may have limitations as they are particularly designed for classification tasks, which are not suitable for dense prediction tasks that usually require effective feature pyramids.

## 5.2. Object Detection

**Experiment Settings.** We conduct object detection experiments on the challenging COCO benchmark [28]. All models are trained on the COCO `train2017` ( $\sim 118k$  images) and evaluated on the `val2017` (5k images). We evaluate our PVT backbones on two standard detectors: RetinaNet [27] and Mask R-CNN [14]. During training, we first use the pre-trained weights on ImageNet to initialize the backbone and Xavier [13] to initialize the newly added layers. Our models are trained with the batch size of 16 on 8 V100 GPUs and optimized by AdamW [33] with the initial learning rate of  $1 \times 10^{-4}$ . Following the common setting [27, 14, 5], we adopt  $1 \times$  or  $3 \times$  training schedule (*i.e.*, 12 or 36 epochs) to train all detection models. The training image is resized to the shorter side of 800 pixels, while the longer side does not exceed 1333 pixels. When using  $3 \times$  training schedule, we also randomly resize the shorter side of the input image within the range of [640, 800]. In the testing phase, the shorter side of the input image is fixed to 800 pixels.

**Results.** As shown in Table 3, using RetinaNet for object detection, we find that when the parameter number is comparable, the PVT variants significantly surpasses their counterparts, showing that our PVT can be a good alternative to the CNN backbone for object detection. For example, with  $1 \times$  training schedule, RetinaNet+PVT-Tiny is 4.9 AP better than RetinaNet+ResNet18 [15] (36.7 vs. 31.8). Moreover, with  $3 \times$  training schedule and multi-scale training, RetinaNet+PVT-Large archive 43.4 AP, surpassing RetinaNet+ResNeXt101-64x4d [56] 41.8 AP, while our parameter number is 30% fewer (71.1M vs. 95.5M).

Similar results are found in the instance segmentation experiment using Mask R-CNN, as shown in Table 4. With  $1 \times$  training schedule, Mask R-CNN+PVT-Tiny achieves 35.1 mask AP ( $AP^m$ ), which is 3.9  $AP^m$  better than Mask R-CNN+ResNet18 and even 0.7  $AP^m$  higher than Mask R-CNN+ResNet50. The best  $AP^m$  obtained by Mask R-CNN+PVT-Large 40.7, which is 1.0  $AP^m$  higher than the model based on ResNeXt101-64x4d.

## 5.3. Semantic Segmentation

**Experiment Settings.** We choose ADE20K [63], a challenging scene parsing benchmark for semantic segmentation. ADE20K contains 150 fine-grained semantic cate-

Backbone	#Param (M)	RetinaNet 1x						RetinaNet 3x + MS					
		AP	AP <sub>50</sub>	AP <sub>75</sub>	AP <sub>S</sub>	AP <sub>M</sub>	AP <sub>L</sub>	AP	AP <sub>50</sub>	AP <sub>75</sub>	AP <sub>S</sub>	AP <sub>M</sub>	AP <sub>L</sub>
ResNet18 [15]	21.3	31.8	49.6	33.6	16.3	34.3	43.2	35.4	53.9	37.6	19.5	38.2	46.8
PVT-Tiny (ours)	23.0	36.7(+4.9)	56.9	38.9	22.6	38.8	50.0	39.4(+4.0)	59.8	42.0	25.5	42.0	52.1
ResNet50 [15]	37.7	36.3	55.3	38.6	19.3	40.0	48.8	39.0	58.4	41.8	22.4	42.8	51.6
PVT-Small (ours)	34.2	40.4(+4.1)	61.3	43.0	25.0	42.9	55.7	42.2(+3.2)	62.7	45.0	26.2	45.2	57.2
ResNet101 [15]	56.7	38.5	57.8	41.2	21.4	42.6	51.1	40.9	60.1	44.0	23.7	45.0	53.8
ResNeXt101-32x4d [56]	56.4	39.9(+1.4)	59.6	42.7	22.3	44.2	52.5	41.4(+0.5)	61.0	44.3	23.9	45.5	53.7
PVT-Medium (ours)	53.9	41.9(+3.4)	63.1	44.3	25.0	44.9	57.6	43.2(+2.3)	63.8	46.1	27.3	46.3	58.9
ResNeXt101-64x4d [56]	95.5	41.0	60.9	44.0	23.9	45.2	54.0	41.8	61.5	44.4	25.2	45.4	54.6
PVT-Large (ours)	71.1	42.6(+1.6)	63.7	45.4	25.8	46.0	58.4	43.4(+1.6)	63.6	46.1	26.1	46.0	59.5

Table 3: **Object detection performance on the COCO val2017.** “#Param” refers to parameter number. “MS” means using multi-scale training [27, 14]

Backbone	#Param (M)	Mask R-CNN 1x						Mask R-CNN 3x + MS					
		AP <sup>b</sup>	AP <sub>50</sub> <sup>b</sup>	AP <sub>75</sub> <sup>b</sup>	AP <sup>m</sup>	AP <sub>50</sub> <sup>m</sup>	AP <sub>75</sub> <sup>m</sup>	AP <sup>b</sup>	AP <sub>50</sub> <sup>b</sup>	AP <sub>75</sub> <sup>b</sup>	AP <sup>m</sup>	AP <sub>50</sub> <sup>m</sup>	AP <sub>75</sub> <sup>m</sup>
ResNet18 [15]	31.2	34.0	54.0	36.7	31.2	51.0	32.7	36.9	57.1	40.0	33.6	53.9	35.7
PVT-Tiny (ours)	32.9	36.7(+2.7)	59.2	39.3	35.1(+3.9)	56.7	37.3	39.8(+2.9)	62.2	43.0	37.4(+3.8)	59.3	39.9
ResNet50 [15]	44.2	38.0	58.6	41.4	34.4	55.1	36.7	41.0	61.7	44.9	37.1	58.4	40.1
PVT-Small (ours)	44.1	40.4(+2.4)	62.9	43.8	37.8(+3.4)	60.1	40.3	43.0(+2.0)	65.3	46.9	39.9(+2.8)	62.5	42.8
ResNet101 [15]	63.2	40.4	61.1	44.2	36.4	57.7	38.8	42.8	63.2	47.1	38.5	60.1	41.3
ResNeXt101-32x4d [56]	62.8	41.9(+1.5)	62.5	45.9	37.5(+1.1)	59.4	40.2	44.0(+1.2)	64.4	48.0	39.2(+0.7)	61.4	41.9
PVT-Medium (ours)	63.9	42.0(+1.6)	64.4	45.6	39.0(+2.6)	61.6	42.1	44.2(+1.4)	66.0	48.2	40.5(+2.0)	63.1	43.5
ResNeXt101-64x4d [56]	101.9	42.8	63.8	47.3	38.4	60.6	41.3	44.4	64.9	48.8	39.7	61.9	42.6
PVT-Large (ours)	81.0	42.9(+0.1)	65.0	46.6	39.5(+1.1)	61.9	42.5	44.5(+0.1)	66.0	48.3	40.7(+1.0)	63.4	43.7

Table 4: **Object detection and instance segmentation performance on the COCO val2017.** “#Param” refers to parameter number. AP<sup>b</sup> and AP<sup>m</sup> denote bounding box AP and mask AP, respectively. “MS” means using multi-scale training [27, 14].

Backbone	Semantic FPN	
	#Param (M)	mIoU (%)
ResNet18 [15]	15.5	32.9
PVT-Tiny (ours)	17.0	35.7(+2.8)
ResNet50 [15]	28.5	36.7
PVT-Small (ours)	28.2	39.8(+3.1)
ResNet101 [15]	47.5	38.8
ResNeXt101-32x4d [56]	47.1	39.7(+0.9)
PVT-Medium (ours)	48.0	41.6(+2.8)
ResNeXt101-64x4d [56]	86.4	40.2
PVT-Large (ours)	65.1	42.1(+1.9)

Table 5: **Semantic segmentation performance of different backbones on the ADE20K validation set.** “#Param” refers to parameter number.

gories, where there are 20210, 2000, and 3352 images for training, validation and, testing, respectively. We evaluate our PVT backbone by applying it to Semantic FPN [21], a simple segmentation method without dilated convolutions [57]. In the training phase, the backbone is initialized with the pre-trained weights on ImageNet [9], and other

newly added layers are initialized with Xavier [13]. We optimize our models by AdamW [33] with the initial learning rate of 1e-4. Following the common settings [21, 6], we train our models for 80k iterations with the batch size of 16 on 4 V100 GPUs. The learning rate is decayed according to the polynomial decay schedule with the power of 0.9. We randomly resize and crop the training image to 512 × 512 and scale the image to the shorter side of 512 during testing.

**Results.** As shown in Table 5, our PVT consistently outperforms ResNet [15] and ResNeXt [56] under different parameter scales, using Semantic FPN for semantic segmentation. For example, with almost the same parameter number, our PVT-Tiny/Small/Medium is at least 2.8 mIoU higher than ResNet-18/50/101. In addition, although the parameter number of our Semantic FPN+PVT-Large is 20% lower than that of Semantic FPN+ResNeXt101-64x4d, the mIoU is still 1.9 higher (42.1 vs. 40.2), showing that for semantic segmentation, our PVT can extract better features than the CNN backbone benefitting from the global attention mechanism.

Method	DETR					
	AP	AP <sub>50</sub>	AP <sub>75</sub>	AP <sub>S</sub>	AP <sub>M</sub>	AP <sub>L</sub>
ResNet50	32.3	53.9	32.3	10.7	33.8	53.0
PVT-Small (ours)	34.7(+2.4)	55.7	35.4	12.0	36.4	56.7

Table 6: **Performance of the pure Transformer object detection pipeline.** We build a pure Transformer detector by combining PVT and DETR [4], whose AP is 2.4 higher than the original DETR based on ResNet50 [15].

Method	#Param (M)	GFLOPs	mIoU (%)
R50-d8+DeeplabV3+	26.8	120.5	41.5
R50-d16+DeeplabV3+	26.8	45.5	40.6
R50-d16+Trans2Seg	56.1	79.3	39.7
PVT-Small+Trans2Seg	32.1	31.6	42.6(+2.9)

Table 7: **Performance of the pure Transformer semantic segmentation pipeline.** We build a pure Transformer detector by combining PVT and Trans2Seg [55]. It is 2.9% higher than ResNet50-d16+Trans2Seg and 1.1% higher than ResNet50-d8+DeeplabV3+ with lower GFLOPs. “d8” and “d16” means dilation 8 and 16, respectively.

#### 5.4. Pure Transformer Dense Prediction

We replace ResNet50 with PVT on DETR [4] for detection and Trans2Seg [55] for segmentation, building pure Transformer dense prediction pipelines. The results prove that fully Transformer without convolution also works well on both object detection and semantic segmentation.

**PVT+DETR.** We build a pure Transformer model for object detection by combining our PVT with DETR [4], which has a Transformer-based detection head. We train models on the COCO train2017 for 50 epochs with the initial learning rate of  $1 \times 10^{-4}$ . The learning rate is divided by 10 at the 33rd epoch. We use random flip and random scale as the data augmentation. All other experiment settings is the same as that of Sec. 5.2. As reported in Table 6, PVT+DETR achieve 34.7 AP on the COCO val2017, outperforming ResNet50+DETR by 2.4 AP (34.7 vs. 32.3).

**PVT+Trans2Seg.** We build a pure Transformer model for semantic segmentation by combining our PVT with Trans2Seg [55], a segmentation head based on Transformer decoder. According to the experiment settings in Sec. 5.3, we perform experiments on ADE20K [63] dataset with 40k iterations training, single scale testing, and compare it with ResNet50+Trans2Seg, DeeplabV3+ with dilation 8 (d8) and 16 (d16), as shown in Table 7.

We find that PVT-Small+Trans2Seg achieves 42.6 mIoU, outperforming ResNet50-d8+DeeplabV3+ (41.5). Note that, ResNet50-d8+DeeplabV3+ has 120.5 GFLOPs due

Method	#Param (M)	RetinaNet 1x		
		AP	AP <sub>50</sub>	AP <sub>75</sub>
ViT-Small/4 [10]	60.9	Out of Memory		
ViT-Small/32 [10]	60.8	31.7	51.3	32.3
PVT-Small (ours)	34.2	40.4	61.3	43.0

Table 8: **Performance comparison between ViT and our PVT using RetinaNet for object detection.** ViT-Small/4 is out of GPU memory due to small patch size (*i.e.*,  $4 \times 4$  per patch). ViT-Small/32 obtain the 31.7 AP on the COCO val2017, which is 8.7 lower than our PVT.

to the high computation cost of dilated convolution, and our PVT-Small+Trans2Seg has only 31.6 GFLOPs. PVT-Small+Trans2Seg also performs better than ResNet50-d16+Trans2Seg (31.6G Flops vs. 79.3 GFLOPs, 42.6 vs. 39.7, only 40% GFLOPs and 2.9 mIoU higher).

#### 5.5. Ablation Study

**Experiment Settings.** We conduct ablation studies on ImageNet [9] and COCO[28] datasets. The experimental settings on ImageNet are the same as the settings in Sec. 5.1. On the COCO dataset, all models are trained using  $1 \times$  training schedule (*i.e.*, 12 epochs), and other experimental settings follow the settings in Sec. 5.2.

**Pyramid Structure.** Pyramid structure is crucial when applying Transformer to dense prediction tasks. Previous ViT is a columnar framework, whose output is single-scale. It raises a problem that when using coarse image patches (*e.g.*,  $32 \times 32$  per patch) as input, the resolution of the output feature map will be low, resulting in poor detection performance (31.7 AP on the COCO val2017), as shown in Table 8. When using fine-grained image patches (*e.g.*,  $4 \times 4$  per patch) as input, ViT will exhaust the GPU memory (*e.g.*, 32G). Differently, our method avoids this problem through a progressive shrinking pyramid. Our method can process high-resolution feature maps in shallow stages and low-resolution feature maps in deep stages. Thus, our method obtains a promising AP of 40.4 on the COCO val2017, 8.7 AP higher than ViT-Small/32 (40.4 vs. 31.7).

**Deeper vs. Wider.** The problem of whether the CNN backbone should go deeper or wider has been extensively discussed in previous work [15, 58]. Here, we explore this problem in our PVT. For fair comparisons, we multiply the hidden dimensions  $\{C_1, C_2, C_3, C_4\}$  of PVT-Small by a scale factor 1.4 to make it have an equivalent parameter number to the deep model (*i.e.*, PVT-Medium). As shown in Table 9, the deep model (*i.e.*, PVT-Medium) consistently works better than the wide model (*i.e.*, PVT-Small-Wide) on both ImageNet and COCO. Therefore, going deeper is more

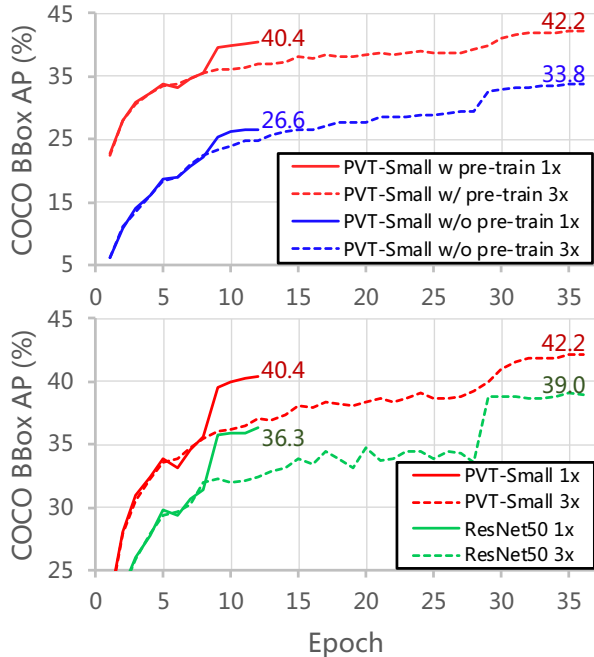


Figure 5: **AP curves of RetinaNet on the COCO val2017 under different backbone settings.** Top: using weights pre-trained on ImageNet vs. random initialization. Bottom: PVT-S vs. R50 [15].

Method	#Param (M)	Top-1	RetinaNet 1x		
			AP	AP <sub>50</sub>	AP <sub>75</sub>
PVT-Small-Wide	46.8	19.3	40.8	61.8	43.3
PVT-Medium	44.2	18.8	41.9	63.1	44.3

Table 9: **Deeper vs. Wider.** “Top-1” denotes the top-1 error on the ImageNet validation set. “AP” denotes the bounding box AP on the COCO val2017. The deep model (*i.e.*, PVT-Medium) obtains better performance than the wide model (*i.e.*, PVT-Small-Wide) under comparable parameter number.

effective than going wider in the design of PVT. Based on this observation, in Table 1, we develop PVT models with different scales by increasing the model depth.

**Pre-trained Weights.** Most dense prediction models (*e.g.*, RetinaNet [27]) rely on the backbone whose weights are pre-trained on ImageNet. We also discuss this problem in our PVT. In the top of Figure 5, we plot the validation AP curves of RetinaNet-PVT-Small w/ (red curves) and w/o (blue curves) pre-trained weights. We find that the model w/ pre-trained weights converges better than the one w/o pre-trained weights, and the gap between their final AP reaches 13.8 under the 1× training schedule and 8.4 under

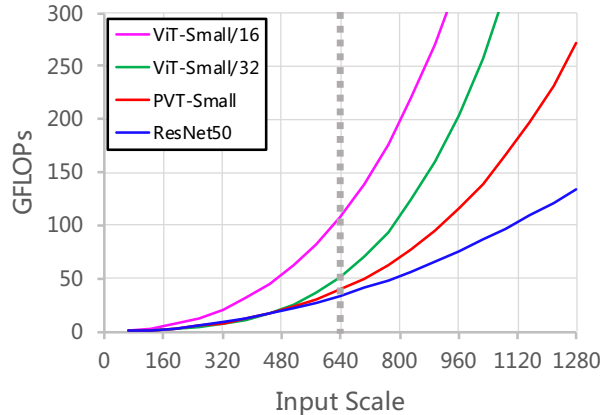


Figure 6: **GFLOPs under different input scales.** The growth rate of GFLOPs: ViT-Small/16 [10] > ViT-Small/32 [10] > PVT-Small > ResNet50 [15]. When the input scale is less than  $640 \times 640$ , the GFLOPs of PVT-Small and ResNet50 [15] are close.

Method	Scale	GFLOPs	Time (ms)	RetinaNet 1x		
				AP	AP <sub>50</sub>	AP <sub>75</sub>
R50 [15]	800	239.3	55.9	36.3	55.3	38.6
PVT-S (ours)	640	157.2	51.7	38.7	59.3	40.8
	800	285.8	76.9	40.4	61.3	43.0

Table 10: **Latency and AP under different input scales.** “Scale” and “Time” denote the input scale and time cost per image. When the shorter side of the input image is 640 pixels, the PVT-S+RetinaNet has lower GFLOPs and time cost than R50 [15]+RetinaNet, while obtaining 2.4 better AP (38.7 vs. 36.3). Note that, the time cost is tested on one V100 GPU with the batch size of 1.

the 3× training schedule and multi-scale training. Therefore, like CNN-based models, pre-training weights can also help PVT-based models converge faster and better. Moreover, in the bottom of Figure 5, we also see that the convergence speed of PVT-based models (red curves) is faster than that of ResNet-based models (green curves).

**Computation Cost.** With the increment of input scale, the growth rate of GFLOPs of our method is greater than ResNet [15], but less than ViT [10], as shown in Figure 6, which means that our PVT is more suitable for tasks with medium-resolution input (*e.g.*, shorter size does not exceed 800 pixels). On COCO, the shorter side of the input image is 800 pixels. Under this condition, the inference speed of RetinaNet based on PVT-Small is slower than the one based on ResNet50, as reported in Table 10.

A direct solution for this problem is to reduce the input scale. When reducing the shorter side of the input image

to 640 pixels, the model based on PVT-Small runs faster than the ResNet50-based model, but our AP is 2.4 higher (38.7 vs. 36.3). Another possible solution is to develop a novel self-attention layer with lower computational complexity for visual tasks. This is a direction worth exploring, and we will pay consistent efforts in it in the future.

## 6. Conclusions and Future Work

In this paper, we introduce PVT, a pure Transformer backbone for dense prediction tasks such as object detection and semantic segmentation. We develop a progressive shrinking pyramid and a spatial-reduction attention layer to obtain multi-scale feature maps under limited computation/memory resources. Extensive experiments on object detection and semantic segmentation benchmarks verify that our PVT is stronger than well-designed CNN backbones under comparable numbers of parameters.

Although PVT can serve as an alternative to the CNN backbone (e.g., ResNet, ResNeXt), there are still some specific modules and operations designed for CNNs but not considered in this work, such as SE [16], SK [24], dilated convolution [57], and NAS [48]. Moreover, with years of rapid developments, there are many well-engineered CNN backbones such as Res2Net [12], EfficientNet [48], and ResNeSt [60]. On the contrary, the Transformer-based model in computer vision is still in its early stage of development. Therefore, we believe there are many potential technologies to be explored in the future. We hope that our method could serve as a good starting point.

## References

- [1] Jimmy Lei Ba, Jamie Ryan Kiros, and Geoffrey E Hinton. Layer normalization. *arXiv preprint arXiv:1607.06450*, 2016. **5**
- [2] Irwan Bello, Barret Zoph, Ashish Vaswani, Jonathon Shlens, and Quoc V Le. Attention augmented convolutional networks. In *Proc. IEEE Int. Conf. Comp. Vis.*, 2019. **3**
- [3] Zhaowei Cai and Nuno Vasconcelos. Cascade r-cnn: Delving into high quality object detection. In *Proc. IEEE Conf. Comp. Vis. Patt. Recogn.*, 2018. **3**
- [4] Nicolas Carion, Francisco Massa, Gabriel Synnaeve, Nicolas Usunier, Alexander Kirillov, and Sergey Zagoruyko. End-to-end object detection with transformers. In *Proc. Eur. Conf. Comp. Vis.*, 2020. **1, 2, 3, 9**
- [5] Kai Chen, Jiaqi Wang, Jiangmiao Pang, Yuhang Cao, Yu Xiong, Xiaoxiao Li, Shuyang Sun, Wansen Feng, Ziwei Liu, Jiarui Xu, et al. Mmdetection: Open mmlab detection toolbox and benchmark. *arXiv preprint arXiv:1906.07155*, 2019. **7**
- [6] Liang-Chieh Chen, George Papandreou, Iasonas Kokkinos, Kevin Murphy, and Alan L Yuille. Deeplab: Semantic image segmentation with deep convolutional nets, atrous convolution, and fully connected crfs. *IEEE Trans. Pattern Anal. Mach. Intell.*, 2017. **3, 8**
- [7] Liang-Chieh Chen, Yukun Zhu, George Papandreou, Florian Schroff, and Hartwig Adam. Encoder-decoder with atrous separable convolution for semantic image segmentation. In *Proc. Eur. Conf. Comp. Vis.*, 2018. **1**
- [8] Yunpeng Chen, Jianan Li, Huaxin Xiao, Xiaojie Jin, Shuicheng Yan, and Jiashi Feng. Dual path networks. *Proc. Advances in Neural Inf. Process. Syst.*, 2017. **3**
- [9] Jia Deng, Wei Dong, Richard Socher, Li-Jia Li, Kai Li, and Li Fei-Fei. Imagenet: A large-scale hierarchical image database. In *Proc. IEEE Conf. Comp. Vis. Patt. Recogn.*, 2009. **1, 8, 9**
- [10] Alexey Dosovitskiy, Lucas Beyer, Alexander Kolesnikov, Dirk Weissenborn, Xiaohua Zhai, Thomas Unterthiner, Mostafa Dehghani, Matthias Minderer, Georg Heigold, Sylvain Gelly, et al. An image is worth 16x16 words: Transformers for image recognition at scale. *Proc. Int. Conf. Learn. Representations*, 2021. **1, 2, 4, 5, 6, 7, 9, 10**
- [11] Mark Everingham, Luc Van Gool, Christopher KI Williams, John Winn, and Andrew Zisserman. The pascal visual object classes (voc) challenge. *Int. J. Comput. Vision*, 88(2):303–338, 2010. **1**
- [12] Shanghua Gao, Ming-Ming Cheng, Kai Zhao, Xin-Yu Zhang, Ming-Hsuan Yang, and Philip HS Torr. Res2net: A new multi-scale backbone architecture. *IEEE Trans. Pattern Anal. Mach. Intell.*, 2019. **11**
- [13] Xavier Glorot and Yoshua Bengio. Understanding the difficulty of training deep feedforward neural networks. In *Proceedings of the thirteenth international conference on artificial intelligence and statistics*, 2010. **7, 8**
- [14] Kaiming He, Georgia Gkioxari, Piotr Dollár, and Ross Girshick. Mask r-cnn. In *Proc. IEEE Int. Conf. Comp. Vis.*, 2017. **1, 3, 6, 7, 8**
- [15] Kaiming He, Xiangyu Zhang, Shaoqing Ren, and Jian Sun. Deep residual learning for image recognition. In *Proc. IEEE Conf. Comp. Vis. Patt. Recogn.*, 2016. **1, 2, 3, 4, 5, 6, 7, 8, 9, 10**
- [16] Jie Hu, Li Shen, and Gang Sun. Squeeze-and-excitation networks. In *Proc. IEEE Conf. Comp. Vis. Patt. Recogn.*, pages 7132–7141, 2018. **11**
- [17] Ronghang Hu and Amanpreet Singh. Transformer is all you need: Multimodal multitask learning with a unified transformer. *arXiv preprint arXiv:2102.10772*, 2211. **2**
- [18] Gao Huang, Zhuang Liu, Laurens Van Der Maaten, and Kilian Q Weinberger. Densely connected convolutional networks. In *Proc. IEEE Conf. Comp. Vis. Patt. Recogn.*, 2017. **3**
- [19] Zilong Huang, Xinggang Wang, Lichao Huang, Chang Huang, Yunchao Wei, and Wenyu Liu. Ccnet: Criss-cross attention for semantic segmentation. In *Proc. IEEE Int. Conf. Comp. Vis.*, 2019. **3**
- [20] Asifullah Khan, Anabia Sohail, Umme Zahoora, and Aqsa Saeed Qureshi. A survey of the recent architectures of deep convolutional neural networks. *Artificial Intelligence Review*, 53(8):5455–5516, 2020. **3**
- [21] Alexander Kirillov, Ross Girshick, Kaiming He, and Piotr Dollár. Panoptic feature pyramid networks. In *Proc. IEEE Conf. Comp. Vis. Patt. Recogn.*, pages 6399–6408, 2019. **1, 3, 6, 8**

- [22] Alex Krizhevsky, Ilya Sutskever, and Geoffrey E Hinton. Imagenet classification with deep convolutional neural networks. *Proc. Advances in Neural Inf. Process. Syst.*, 2012. **3**
- [23] Yann LeCun, Léon Bottou, Yoshua Bengio, and Patrick Haffner. Gradient-based learning applied to document recognition. 1998. **3**
- [24] Xiang Li, Wenhai Wang, Xiaolin Hu, and Jian Yang. Selective kernel networks. In *Proc. IEEE Conf. Comp. Vis. Patt. Recogn.*, 2019. **3, 11**
- [25] Xiang Li, Wenhai Wang, Lijun Wu, Shuo Chen, Xiaolin Hu, Jun Li, Jinhui Tang, and Jian Yang. Generalized focal loss: Learning qualified and distributed bounding boxes for dense object detection. In *Proc. Advances in Neural Inf. Process. Syst.*, 2020. **3**
- [26] Tsung-Yi Lin, Piotr Dollár, Ross Girshick, Kaiming He, Bharath Hariharan, and Serge Belongie. Feature pyramid networks for object detection. In *Proc. IEEE Conf. Comp. Vis. Patt. Recogn.*, 2017. **3, 6**
- [27] Tsung-Yi Lin, Priya Goyal, Ross Girshick, Kaiming He, and Piotr Dollár. Focal loss for dense object detection. In *Proc. IEEE Int. Conf. Comp. Vis.*, 2017. **1, 2, 3, 6, 7, 8, 10**
- [28] Tsung-Yi Lin, Michael Maire, Serge Belongie, James Hays, Pietro Perona, Deva Ramanan, Piotr Dollár, and C Lawrence Zitnick. Microsoft coco: Common objects in context. In *Proc. Eur. Conf. Comp. Vis.*, 2014. **1, 7, 9**
- [29] Chenxi Liu, Liang-Chieh Chen, Florian Schroff, Hartwig Adam, Wei Hua, Alan L Yuille, and Li Fei-Fei. Auto-deeplab: Hierarchical neural architecture search for semantic image segmentation. In *Proc. IEEE Conf. Comp. Vis. Patt. Recogn.*, 2019. **3**
- [30] Wei Liu, Dragomir Anguelov, Dumitru Erhan, Christian Szegedy, Scott Reed, Cheng-Yang Fu, and Alexander C Berg. Ssd: Single shot multibox detector. In *Proc. Eur. Conf. Comp. Vis.*, 2016. **3**
- [31] Jonathan Long, Evan Shelhamer, and Trevor Darrell. Fully convolutional networks for semantic segmentation. In *Proc. IEEE Conf. Comp. Vis. Patt. Recogn.*, 2015. **3**
- [32] Ilya Loshchilov and Frank Hutter. Sgdr: Stochastic gradient descent with warm restarts. *arXiv preprint arXiv:1608.03983*, 2016. **7**
- [33] Ilya Loshchilov and Frank Hutter. Decoupled weight decay regularization. *arXiv preprint arXiv:1711.05101*, 2017. **7, 8**
- [34] Hyeonwoo Noh, Seunghoon Hong, and Bohyung Han. Learning deconvolution network for semantic segmentation. In *Proc. IEEE Int. Conf. Comp. Vis.*, 2015. **3**
- [35] Prajit Ramachandran, Niki Parmar, Ashish Vaswani, Irwan Bello, Anselm Levskaya, and Jonathon Shlens. Stand-alone self-attention in vision models. *arXiv preprint arXiv:1906.05909*, 2019. **2, 3**
- [36] Shaoqing Ren, Kaiming He, Ross Girshick, and Jian Sun. Faster r-cnn: Towards real-time object detection with region proposal networks. In *Proc. Advances in Neural Inf. Process. Syst.*, 2015. **1, 3**
- [37] Olaf Ronneberger, Philipp Fischer, and Thomas Brox. U-net: Convolutional networks for biomedical image segmentation. In *International Conference on Medical image computing and computer-assisted intervention*, 2015. **3**
- [38] Olga Russakovsky, Jia Deng, Hao Su, Jonathan Krause, Sanjeev Satheesh, Sean Ma, Zhiheng Huang, Andrej Karpathy, Aditya Khosla, Michael Bernstein, et al. Imagenet large scale visual recognition challenge. *Int. J. Comput. Vision*, 2015. **3, 6**
- [39] Suyash Shetty. Application of convolutional neural network for image classification on pascal voc challenge 2012 dataset. *arXiv preprint arXiv:1607.03785*, 2016. **3**
- [40] Connor Shorten and Taghi M Khoshgoftaar. A survey on image data augmentation for deep learning. *Journal of Big Data*, 6(1):1–48, 2019. **3**
- [41] Karen Simonyan and Andrew Zisserman. Very deep convolutional networks for large-scale image recognition. *arXiv preprint arXiv:1409.1556*, 2014. **1, 2, 3**
- [42] Peize Sun, Yi Jiang, Enze Xie, Zehuan Yuan, Changhu Wang, and Ping Luo. Onenet: Towards end-to-end one-stage object detection. *arXiv preprint arXiv:2012.05780*, 2020. **3**
- [43] Peize Sun, Yi Jiang, Rufeng Zhang, Enze Xie, Jinkun Cao, Xinting Hu, Tao Kong, Zehuan Yuan, Changhu Wang, and Ping Luo. Transtrack: Multiple-object tracking with transformer. *arXiv preprint arXiv:2012.15460*, 2020. **2**
- [44] Peize Sun, Rufeng Zhang, Yi Jiang, Tao Kong, Chenfeng Xu, Wei Zhan, Masayoshi Tomizuka, Lei Li, Zehuan Yuan, Changhu Wang, et al. Sparse r-cnn: End-to-end object detection with learnable proposals. *arXiv preprint arXiv:2011.12450*, 2020. **3**
- [45] Christian Szegedy, Sergey Ioffe, Vincent Vanhoucke, and Alexander Alemi. Inception-v4, inception-resnet and the impact of residual connections on learning. In *Proc. AAAI Conf. Artificial Intell.*, 2017. **3**
- [46] Christian Szegedy, Wei Liu, Yangqing Jia, Pierre Sermanet, Scott Reed, Dragomir Anguelov, Dumitru Erhan, Vincent Vanhoucke, and Andrew Rabinovich. Going deeper with convolutions. In *Proc. IEEE Conf. Comp. Vis. Patt. Recogn.*, 2015. **3, 7**
- [47] Christian Szegedy, Vincent Vanhoucke, Sergey Ioffe, Jon Shlens, and Zbigniew Wojna. Rethinking the inception architecture for computer vision. In *Proc. IEEE Conf. Comp. Vis. Patt. Recogn.*, 2016. **3, 7**
- [48] Mingxing Tan and Quoc Le. Efficientnet: Rethinking model scaling for convolutional neural networks. In *Proc. Int. Conf. Mach. Learn.*, 2019. **11**
- [49] Zhi Tian, Chunhua Shen, Hao Chen, and Tong He. Fcos: Fully convolutional one-stage object detection. In *Proc. IEEE Int. Conf. Comp. Vis.*, 2019. **3**
- [50] Hugo Touvron, Matthieu Cord, Matthijs Douze, Francisco Massa, Alexandre Sablayrolles, and Hervé Jégou. Training data-efficient image transformers & distillation through attention. *arXiv preprint arXiv:2012.12877*, 2020. **4, 6, 7**
- [51] Ashish Vaswani, Noam Shazeer, Niki Parmar, Jakob Uszkoreit, Llion Jones, Aidan N Gomez, Lukasz Kaiser, and Illia Polosukhin. Attention is all you need. *arXiv preprint arXiv:1706.03762*, 2017. **2, 4, 5**
- [52] Wenhai Wang, Xiang Li, Jian Yang, and Tong Lu. Mixed link networks. *Proc. Int. Joint Conf. Artificial Intell.*, 2018. **3**

- [53] Xiaolong Wang, Ross Girshick, Abhinav Gupta, and Kaiming He. Non-local neural networks. In *Proc. IEEE Conf. Comp. Vis. Patt. Recogn.*, 2018. [2](#), [3](#)
- [54] Enze Xie, Peize Sun, Xiaoge Song, Wenhai Wang, Xuebo Liu, Ding Liang, Chunhua Shen, and Ping Luo. Polarmask: Single shot instance segmentation with polar representation. In *Proc. IEEE Conf. Comp. Vis. Patt. Recogn.*, pages 12193–12202, 2020. [3](#)
- [55] Enze Xie, Wenjia Wang, Wenhai Wang, Peize Sun, Hang Xu, Ding Liang, and Ping Luo. Segmenting transparent object in the wild with transformer. *arXiv preprint arXiv:2101.08461*, 2021. [2](#), [9](#)
- [56] Saining Xie, Ross Girshick, Piotr Dollár, Zhuowen Tu, and Kaiming He. Aggregated residual transformations for deep neural networks. In *Proc. IEEE Conf. Comp. Vis. Patt. Recogn.*, 2017. [1](#), [2](#), [3](#), [6](#), [7](#), [8](#)
- [57] Fisher Yu and Vladlen Koltun. Multi-scale context aggregation by dilated convolutions. *arXiv preprint arXiv:1511.07122*, 2015. [8](#), [11](#)
- [58] Erwan Zerhouni, Dávid Lányi, Matheus Viana, and Maria Gabrani. Wide residual networks for mitosis detection. In *2017 IEEE 14th International Symposium on Biomedical Imaging*, pages 924–928. IEEE, 2017. [9](#)
- [59] Hongyi Zhang, Moustapha Cisse, Yann N Dauphin, and David Lopez-Paz. mixup: Beyond empirical risk minimization. *arXiv preprint arXiv:1710.09412*, 2017. [7](#)
- [60] Hang Zhang, Chongruo Wu, Zhongyue Zhang, Yi Zhu, Zhi Zhang, Haibin Lin, Yue Sun, Tong He, Jonas Mueller, R Manmatha, et al. Resnest: Split-attention networks. *arXiv preprint arXiv:2004.08955*, 2020. [11](#)
- [61] Hengshuang Zhao, Jiaya Jia, and Vladlen Koltun. Exploring self-attention for image recognition. In *Proc. IEEE Conf. Comp. Vis. Patt. Recogn.*, pages 10076–10085, 2020. [2](#)
- [62] Hengshuang Zhao, Jianping Shi, Xiaojuan Qi, Xiaogang Wang, and Jiaya Jia. Pyramid scene parsing network. In *Proc. IEEE Conf. Comp. Vis. Patt. Recogn.*, 2017. [3](#)
- [63] Bolei Zhou, Hang Zhao, Xavier Puig, Sanja Fidler, Adela Barriuso, and Antonio Torralba. Scene parsing through ade20k dataset. In *Proc. IEEE Conf. Comp. Vis. Patt. Recogn.*, 2017. [1](#), [7](#), [9](#)
- [64] Xizhou Zhu, Weijie Su, Lewei Lu, Bin Li, Xiaogang Wang, and Jifeng Dai. Deformable detr: Deformable transformers for end-to-end object detection. *arXiv preprint arXiv:2010.04159*, 2020. [2](#), [3](#), [4](#)